Synthesis, structural and magnetic characterization of lead-metaniobate/cobalt-ferrite nanocomposite films deposited by pulsed laser ablation

P. Sá[a], J. Barbosa[a], I.T. Gomes[a,c], J.A. Mendes[a,b], J. Ventura[c], J.P. Araújo[c], B.G. Almeida[a]

[a]Centro de Física e Departamento de Física, Universidade do Minho, Campus de Gualtar, 4710-057 Braga, Portugal.

[b]ESEIG, Instituto Politécnico Porto, Rua D. Sancho I, 981, 4480-876 Vila do Conde, Portugal

[c]Departamento de Física and IFIMUP-IN, Institute of Nanoscience and Nano-technology, Universidade do Porto, Rua do Campo Alegre 687, 4169-007 Porto, Portugal

Abstract

Detailed structural, microstructural and magnetic measurements were performed on $(PbNb_2O_6)_{1-x}$-$(CoFe_2O_4)_x$ nanocomposite thin films deposited by laser ablation on Si(001)\Pt substrates, with different ferrite concentrations. The tuning of the lead concentration, due to the lead volatility, was found to be particularly important in order to obtain the orthorhombic (ferroelectric) lead niobate phase. The lattice parameter of $CoFe_2O_4$ was below the bulk value, indicating the presence of compressive strains on this phase. A magnetic anisotropy was observed, which favored the orientation of the magnetization in the direction perpendicular to the plane of the films, for cobalt ferrite concentrations 40-50%. The shape, stress and magnetocrystalline anisotropy fields on the composites were calculated and compared. It was found that the perpendicular magnetic anisotropy was induced by the presence of strain on the ferrite phase in the films.

Keywords: Lead Niobate/Cobalt Ferrite composites, multiferroic thin films, laser ablation, structure, magnetic properties

*Corresponding author: bernardo@fisica.uminho.pt, tel: +351253604063, fax: +351253604079

1. Introduction

Multiferroic piezoelectric-magnetostrictive composites have been recently attracting much scientific and technological interest [1-3]. Due to the mechanical interaction between both phases, these composites present product properties that are not characteristic of each of the individual ones. Besides possessing ferroelectricity and magnetism in the constituent materials, they are shown to exhibit a coupling between their magnetic and electric degrees of freedom, the so called magnetoelectric effect [1-4]. Possible applications include actuators or sensors where the ability to couple either to the electric or the magnetic polarization could be exploited [1], transducers where the magnetization is controlled by an electric field or memory devices [4] (where data could be written electrically and read magnetically). In this type of composites, it is the elastic interaction between the piezoelectric and magnetostrictive materials that provides the coupling mechanism inducing the magnetoelectric response [3]. As a result, the magnetic properties of these nanostructures depend on the phase morphology and internal stress distribution, which, in turn, are determined by the elastic phase/phase interactions. Cobalt ferrite ($CoFe_2O_4$ - magnetostrictive) has previously been used for the development of composite nanostructures, such as nanopillars embedded in a ferroelectric matrix or mulitlayered ferroelectric-ferromagnetic thin films, and these have been shown to present a significant coupling between ferroelectricity and ferromagnetism [3]. Here, thin film composites consisting on cobalt ferrite grains dispersed in a lead niobate matrix ($PbNb_2O_6$ - PNO - piezoelectric) were prepared by laser ablation, with different cobalt ferrite concentrations. The aim is to study the deposition, structure and microstructure of the composite films and its influence on their magnetic properties, in particular, on the origin of the perpendicular magnetic anisotropy here observed at intermediate ferrite concentrations.

Lead metaniobate ($PbNb_2O_6$) is a good candidate for high temperature applications, due to its high ferroelectric Curie temperature (570ºC; higher than on, *e.g.*, barium titanate or

PZT), low mechanical quality factor and large anisotropy in the electromechanical coupling coefficient [5,6]. At temperatures above 1200ºC it has a tetragonal tungsten bronze structure. Upon cooling below 1200ºC it transforms to a rhombohedral form that is paraelectric at room temperature. If the cooling through the 1200ºC-700ºC interval is fast, the tetragonal phase is retained down to 570ºC where it changes to a ferroelectric orthorhombic metastable structure [6]. In thin film form, the ferroelectric orthorhombic led niobate phase can be stabilized at lower temperatures (450-900ºC [7-9]) as compared to ceramics. However, care must be taken on the stabilization of the ferroelectric orthorhombic phase, due to the possible formation of residual non-ferroelectric phases during deposition [8,9].

$CoFe_2O_4$ has a cubic inverse spinel structure [10] in which the octahedral B sites are occupied by eight Co^{2+} and eight Fe^{3+} cations, while the tetrahedral A sites are occupied by the remaining eight Fe^{3+}. It is a ferrimagnetic material with a Curie temperature of 520 ºC [10,11] and a saturation magnetization of 425 emu/cm^3 at room temperature [11]. Additionally, it presents a high magnetocrystalline anisotropy and magnetostriction [10], making it suitable for application in multiferroic composite thin films.

2. Experimental

The $(PbNb_2O_6)_{1-x}$-($CoFe_2O_4)_x$ thin films were prepared by laser ablation, on platinum covered Si(001) substrates. The depositions were done with a KrF excimer laser (wavelength λ = 248 nm), at a fluence of 2 J/cm^2. The pulse duration of the laser was 25 ns and the repetition rate was 10 Hz. The films were deposited in a reactive oxygen atmosphere, with an oxygen pressure of 0.2 mbar. The substrate temperature was 600ºC. The ablation targets were produced by mixing cobalt ferrite and lead niobate powders with cobalt ferrite weight concentrations of x = 0% (pure $PbNb_2O_6$), 10%, 30%, 40%, 50%, 70%, 90% and 100% (pure $CoFe_2O_4$). They were then compressed and sintered at 1100ºC during 8 hour. To compensate

for the high volatility of lead during deposition [8,12], the lead niobate powders (and, correspondingly, the targets) presented $PbNb_2O_6$ mixed with a small amount of lead niobate phases with excess lead ($Pb_3Nb_4O_{13}$).

The structural studies were performed by X-ray diffraction (XRD), using a Philips PW-1710 diffractometer with CuKα radiation. The X-ray diffraction θ-2θ measurements were performed by rotating the sample surface an angle θ relative to the incident beam while simultaneously rotating the detector by an angle 2θ. Thus, the incident and the scattered angles relative to the sample plane were always equal to each other, so that the diffraction vector $\mathbf{q} = \mathbf{k'} - \mathbf{k}$ was always perpendicular to the samples surface (**k** and **k'** are the incident and scattered wavevectors of the X-ray beams). With this measurement configuration, the resulting diffraction spectra correspond to scans of the structure perpendicular to the films plane and, as such, along their growth direction. Also, after mounting each sample, and prior to the diffraction measurements, a calibration of the diffractometer angles was performed using the substrate Si(004) peak position as reference.

The Raman studies were performed using a Jobin-Yvon T64000 spectrometer with an excitation wavelength at 514.5 nm, from an Ar laser. Scanning electron microscopy (SEM) was performed with a Nova NanoSEM 200 microscope. The magnetic properties were measured with a Quantum Design MPMS SQUID magnetometer.

3. Results

3.1. Structural characterization

Figures 1a)-1c) show the X-ray diffraction spectra measured on films prepared with a temperature of 600ºC. They were deposited with a target-substrate distance of 3 cm. The vertical lines mark the peak positions of bulk lead niobate ($PbNb_2O_6$) with the orthorhombic

phase [13]. The open circles indicate the corresponding peak positions of the $Pb_3Nb_4O_{13}$ phase with the cubic structure, while the lozenges mark the peak positions of bulk $CoFe_2O_4$ with the cubic spinel structure [13]. The films are polycrystalline and composed by $PbNb_2O_6$ with the orthorhombic structure and $CoFe_2O_4$ with cubic spinnel phase. An excess-lead $Pb_3Nb_4O_{13}$ (relative to $PbNb_2O_6$), non-ferroelectric cubic lead-niobate phase, that was present on the targets, is also present on the films.

In order to optimize the deposition conditions and reduce the residual $Pb_3Nb_4O_{13}$ phase on the films, they were deposited at different substrate-target distances (d_{ST}), while the remaining deposition parameters, in particular oxygen pressure and substrate temperature, were kept constant, since they already induced the presence of the orthorhombic phase in the films. In fact, due to the high volatility of lead [8,12] it is expected that it presents a lower concentration on the plume front, as the target-substrate distance increases. Then, for larger distances the amount of the lead-excess residual phase should be reduced. In fact, as shown on X-ray diffraction spectra of figures 1d)-1g), for the particular case of the films deposited with 10% cobalt ferrite concentration, as d_{ST} increases the proportion of the lead-excess PNO phase is strongly reduced so that for d_{ST} = 10 cm only the orthorhombic $PbNb_2O_6$ phase is present. As such, the subsequent films were deposited with d_{ST} = 9 cm.

The X-ray diffraction peaks were fitted with Gaussian functions in order to determine peak positions and widths. To improve the fitting results, several different fits to the diffraction peaks, using different initial parameters, were used in order to ascertain the convergence of the solution. The lattice parameters were obtained from the calculated peak positions of the (350),(530) peaks (at 29.2 ° and 30.4º, respectively) for PNO and of the (311) peak for $CoFe_2O_4$. For the $PbNb_2O_6$ phase, the calculated lattice parameters (e.g. *a* is near 17.6Å, *b* is around 18.0 Å) are near but higher than the bulk values [13] indicating the presence of an expansion strain on this phase in the films. On the other hand, for the $CoFe_2O_4$

phase the lattice parameter $a_{CoFe2O4,film}$ was in the range from 8.32 Å, on the intermediate ferrite concentrations, to 8.37 Å, slightly lower than the bulk value $a_{CoFe2O4,film}$ = 8.39 Å, indicating that this phase was strained (compressed) in the films. Since, the diffraction vector of the θ-2θ X-ray diffraction measurements performed on the samples (fig. 1), scanned a direction perpendicular to the films plane (and, thus, parallel to the growth direction), then, this indicates that the observed cobalt ferrite lattice planes compression and the lead niobate expansion is along the growth direction of the films. This, in turn, indicates the presence of in-plane tensile and compressive stresses on the CFO and PNO phases in the films, respectively. The grain size, estimated from the X-ray diffraction peak widths using the Scherrer equation [14,15], was ~25 mn for the lead niobate phase and ~8 nm for the cobalt ferrite one, on the samples.

To characterize the micro- and nanostructure and, in particular, the distribution of grain sizes in the nanocomposites, scanning electron microscopy (SEM) measurements were performed on the samples surface. Figure 2a) show a SEM micrograph for the particular case of the film with x = 10%, deposited with d_{ST} = 9 cm. The films surface shows a granular morphology with aggregates of grains of different sizes. The number of grains with a diameter falling on a particular range was determined from the images and histograms were made in order to obtain their size distribution. Figure 2b) shows the corresponding histogram obtained from the SEM micrograph of figure 2a). The grain size distribution was calculated by fitting the histogram with two Gaussian functions: one corresponding to the smaller sizes and the other to the higher ones (fig. 2b). The average grain size of the smaller grains was 12 nm, with a distribution width (full wide half maximum – FWHM) of 13 nm. The average grain size of the larger ones was 21 nm, with a distribution width of 4 nm. Consistent with the X-ray results, the smaller sized grains, with 12 nm average size, correspond mainly to the cobalt ferrite, while the larger ones, with 21 nm average size, correspond to the lead niobate phase.

The samples thicknesses were obtained from SEM micrographs measured transverse to the sample surface, giving thicknesses of 80-100 nm.

3.2 Raman spectroscopy

To further characterize the films and, in particular, the cobalt ferrite phase on them, Raman spectroscopy measurements were performed on the samples. Raman spectroscopy yields phonon parameters reflecting the local crystal symmetry, allowing the study of the nanograins structure. Figure 3 shows the Raman spectra of the thin films deposited with cobalt ferrite concentrations in the range 10%-70%. Also shown are the individual $PbNb_2O_6$ ($x = 0\%$) and $CoFe_2O_4$ ($x = 100\%$) bulk reference powders, for comparison.

On the films, several bands of the lead niobate and $CoFe_2O_4$ phases are observed on the spectra and their positions are represented by full lines and dotted lines in figure 3, respectively. Based on the peaks observed on the powders, the nanocomposite films spectra were deconvoluted by using Lorentzian line-shape functions to least-squares fit the Raman peaks. Figure 3 shows the fitted lorentzians for the particular case where the concentration of the cobalt ferrite is $x = 30\%$. From the fitted lorentzians, the vibrational modes wavenumber was determined by the peak positions. For the $CoFe_2O_4$ phase, two bands are more clearly visible. The corresponding fitted lozentzians give wavenumbers in the 455-465 cm^{-1} and 660-675 cm^{-1} regions, for these peaks, depending on the concentration.

The spinel ferrite structure of $CoFe_2O_4$ has the space group $Fd\bar{3}m$ (O_g^7) and factor group analysis predicts five Raman active modes, namely, one A_{1g}, one E_g and three F_{2g} modes [16-18]. The active Raman modes are at 210cm^{-1} (F_{2g}), 305cm^{-1} (E_g), 466cm^{-1} (F_{2g}), 577cm^{-1} (F_{2g}) and 695cm^{-1} (A_{1g}) [17]. Then, the cobalt ferrite modes appearing at 455-465 cm^{-1} and 660-675 cm^{-1} can be assigned to the F_{2g} and to the A_{1g} vibration modes, respectively. The ferrite modes observed on the thin films are consistent with the spinel ferrite structure as

was also observed on the X-ray results. The slightly different peak positions between the bands of $CoFe_2O_4$ on the films and the corresponding ones on the bulk reference powder indicate the presence of strains [19] on the cobalt ferrite phase, as already observed on the X-ray diffraction results of the films.

3.3 Magnetic characterization

Figure 4a)-4d) shows the magnetization hysteresis cycles measured at ambient temperature on the nanocomposites with x = 30%, 40%, 50% and 70%, respectively. The loops were obtained with the magnetic field (H) applied perpendicular and parallel to the films plane. They were corrected by subtracting the diamagnetic contribution from the substrate. The increase of the saturation magnetization with increasing ferrite content is due to the decreasing concentration of the non-magnetic lead metaniobate phase on the samples. By normalizing to the ferrite concentration, the saturation magnetization of the magnetic phase in the films is ~ 400 emu/cm^3, near the bulk value of 425 emu/cm^3.

For the films with higher and lower ferrite concentration the hysteresis cycles for the perpendicular-to-the-plane and parallel-to-the-plane applied magnetic fields are similar, indicating a low degree of magnetic anisotropy and evidencing the random character of the alignment of the magnetization of the films. However, for the films with intermediate cobalt ferrite content (40%-50%), particularly on the one with x = 50 %, the magnetization loops measured with an in-plane applied H field (H∥plane) are harder to saturate, while the loops measured with an H field applied perpendicular to the plane (H⊥plane) reach saturation at lower magnetic fields. This indicates the presence of an anisotropy favouring the orientation of the magnetization in the direction perpendicular to the films plane. Considering an uniaxial anisotropy with the magnetization easy axis perpendicular to the plane, the anisotropy fields (H_A) can be obtained from the hard-axis saturation field (H∥plane loop) [10]. Thus, by

determining the magnetic field at which the saturation magnetization of the out-of-plane magnetization loop (easy axis) intersects the in-plane curve (hard axis), the anisotropy fields (H_A) were found and are shown in figure 5. On this type of composites, the ferrite content where the mechanical interaction between both phases induces a strong magnetoelectric behaviour is on the 40%-50% interval [1,3]. Here, this is the concentration region where the magnetic anisotropy is bigger, indicating that strains and the magnetostriction of the ferrite need to be taken into account.

4. Discussion

To understand the cause of the perpendicular magnetic anisotropy of the polycrystalline films several origins of magnetic anisotropy must be considered, namely, the shape anisotropy, the magnetocrystalline anisotropy and the strain induced anisotropy due to the magnetostriction of $CoFe_2O_4$ [10,20]. In fact, magnetostriction may play an important role in the magnetic behavior, due to strain on the films [20,21].

For a cubic crystal, and an epitaxial film, the magnetocrystalline anisotropy field is determined by $H_K = 2K_1/M_S$, where K_1 is the crystal anisotropy constant [10]. In $CoFe_2O_4$ $K_1 = 3\times10^6$ erg/cm^3 [21], giving H_K near 13 kOe for the thin films (fig. 5). However, due to the random character of the polycrystalline films, and, thus, the random orientation of the magnetic moments of the grains, it is not expected to be the dominant contribution to the magnetic anisotropy. This is observed, in particular, on the films with higher and lower ferrite concentration (figs. 4,5) where the corresponding anisotropy field H_A is small.

To determine the shape anisotropy field due to the dispersion of the $CoFe_2O_4$ magnetic particles in the non-magnetic matrix, an effective magnetostatic energy is calculated as a combination of an isolated particle with demagnetization factor N_P and a homogeneous film with demagnetization factor $N_F = 4\pi$ [22-24]. Considering spherical cobalt ferrite particles

with $N_P = 4\pi/3$, saturation magnetization M_S and volume fraction f_P, the shape anisotropy energy becomes:

$$E_d = (1 - f_p)\, N_p \frac{M_S^2}{2} + f_p\, N_F \frac{M_S^2}{2} \qquad (1)$$

Then, the shape anisotropy field is obtained by $H_d = 2E_d/M_S$ and the corresponding values for the composites are represented in figure 5. The values thus obtained are much lower and cannot explain the experimentally determined perpendicular anisotropy, as shown in figure 5.

In order to determine the strain induced anisotropy field, the magnetostriction coefficients (λ_{100} and λ_{111}) of the cubic cobalt ferrite must be considered. Additionally, for a polycrystalline material containing a random distribution of crystallites an averaged effective saturation magnetostriction (λ_S) coefficient can be determined by [10]:

$$\lambda_S = \frac{2\lambda_{100} + 3\lambda_{111}}{5} \qquad (2)$$

The corresponding anisotropy energy for a polycrystalline sample is then obtained from [10]:

$$E_\sigma = -\frac{3}{2}\lambda_s \sigma \cos^2(\varphi) \qquad (3)$$

where σ is the stress and φ is the angle between the magnetization and the stress. Then, the stress induced anisotropy field H_σ is obtained by $H_\sigma = 2E_\sigma/M_S = 3\lambda_S\sigma/M_S$ [10,21]. For cubic $CoFe_2O_4$ $\lambda_{100} = -5.9\times10^{-4}$ and $\lambda_{111} = 1.2\times10^{-4}$ [10], so that, from equation (2), the saturation magnetostriction coefficient is $\lambda_S = -1.64\times10^{-4}$ for the films. The in-plane stress can be obtained from $\sigma = -\frac{Y}{2\alpha}\varepsilon$ [25] ($\sigma_1 = \sigma_2 = \sigma$) where the strain is $\varepsilon = (a_{CoFe2O4,film} - a_{CoFe2O4,bulk})/a_{CoFe2O4,bulk}$; $a_{CoFe2O4,film}$ is the lattice parameter determined from the (311) peak position, Y is the Young's modulus and α is the Poisson coefficient of the Co-ferrite

($Y = 1.5\times10^2$ GPa, α=0.22 [21,26] at room temperature). The obtained H_σ values are represented in figure 5, and are similar to the experimental ones for the perpendicular anisotropy fields H_A.

One can then understand the origin of the perpendicular magnetic anisotropy observed on the thin films. Since the cobalt ferrite in the films is strained in the growth direction, as obtained by the X-ray diffraction measurements, this indicates the presence of in-plane tensions on the CFO phase (σ positive). Then, due to the negative effective magnetostriction of the cobalt ferrite in the nanocomposites, E_σ is positive and it is only minimized when the angle φ between the magnetization and stress is $\pi/2$ (equation 3). Thus, in order to minimize the strain anisotropy energy the in-plane tensions induce a tendency to align the magnetization in a direction perpendicular to them and, consequently, perpendicular to the plane of the films. This then leads to the appearance of the observed perpendicular anisotropy

Conclusions

$PbNb_2O_6$-$CoFe_2O_4$ nanocomposites have been deposited by laser ablation on Si\Pt substrates and their structural and magnetic properties were characterized. The control and tuning of the lead concentration, due to the lead volatility, was found to be particularly important in order to attain the orthorhombic lead niobate (ferroelectric) phase. On the other hand, the cobalt ferrite phase was under compressing strain in the films, as compared to the bulk. A perpendicular magnetic anisotropy, with a characteristic field H_A at intermediate (40%-50%) $CoFe_2O_4$ concentration was observed in the films. The shape, stress and magnetocrystalline anisotropy fields were determined and compared with H_A. It was found that the perpendicular anisotropy was mainly due to strains developed on the cobalt-ferrite phase, on the nanocomposite films.

Acknowledgments

This work has been supported by Fundação para a Ciência e Tecnologia (FCT) and FEDER, through the projects POCI/CTM/60181/2004 and PTDC/CTM/099415/2008. J. Barbosa and I.T. Gomes gratefully acknowledge PhD grants from Fundação para a Ciência e Tecnologia (SFRH/BD/41913/2007 and SFRH/BD/36348/2007, respectively).

References

[1] J. Ma, J. Hu, Z. Li and C-W Nan, Adv. Mater. 23, 1062 (2011)

[2] J.H. Lee, L. Fang, E. Vlahos, X. Ke, Y.W. Jung, L.F. Kourkoutis, J-W Kim, P.J. Ryan, T. Heeg, M. Roeckerath, V. Goian, M. Bernhagen, R. Uecker, P.C. Hammel, K.M. Rabe, S. Kamba, J. Schubert, J.W. Freeland, D.A. Muller, C.J. Fennie, P. Schiffer, V. Gopalan, E. Johnston-Halperin and D.G. Schlom, Nature 446, 954 (2010)

[3] C.A.F. Vaz, J. Phys.: Condens. Matter 24, 333201 (2012)

[4] H. Béa, M. Gajek, M .Bibes and A. Barthélémy, J. Phys.: Condens. Matter. 20, 434221 (2008)

[5] M. Allahverdi, A. Hall, R. Brennan, M.E. Ebrahimi, N. Marandian Hagh and A. Safari, J. Electroceram. 8, 129 (2002)

[6] A.J. Moulson, J.M. Herbert, Electroceramics: materials, properties and applications, Chapman and Hall, London, 1997

[7] J.M. Xue, S. Ezhilvalavan, X.S. Gao and J. Wang, Appl. Phys. Lett. 81, 877 (2002)

[8] F. Cardoso, B.G. Almeida, P. Caldelas, J.A. Mendes, J. Barbosa, Ferroelectrics 335, 201 (2006)

[9] C.V.R. Vasant Kumar, M. Sayer and R. Pascual, Appl. Phys. Lett. 60, 2207 (1992)

[10] S. Chikazumi, Physics of Ferromagnetism, Oxford University Press, New York, 1997

[11] V.J. Folen, in 6.1.8.1 Co ferrite. ed. K.-H. Hellwege, A.M. Hellwege, SpringerMaterials - The Landolt-Börnstein Database (http://www.springermaterials.com). DOI: 10.1007/10201438_113

[12] O. Auciello, R. Dat, R. Ramesh, in Ferroelectric Thin Films: Synthesis and Basic Properties, ed. C. Paz de Araujo, J.F. Scott, G.W. Taylor, Gordon and Breach, 1996

[13] Powder Diffraction File, Joint Committee on Powder Diffraction Standards, International Centre for Diffraction Data, Cards 11-122 ($PbNb_2O_6$ - orthorhombic), 25-443 ($Pb_3Nb_4O_{13}$ - cubic). 22-1086 ($CoFe_2O_4$ - cubic spinel), (2004)

[14] B.D. Cullity, S.R. Stock, Elements of X-Ray Diffraction, Prentice Hall, 2001

[15] B.G. Almeida, A. Pietka, P. Caldelas, J.A. Mendes and J.L. Ribeiro, Thin Solid Films, 513, 275 (2006)

[16] T. Yu, Z.X. Shen, Y. Shi and J. Ding, J. Phys.: Condens. Matter. 14, L613 (2002)

[17] M. Foerster, M. Iliev, N. Dix, X. Martí, M. Barchuk, F. Sánchez and J. Fontcuberta, Adv. Funct. Mater. 22, 4344 (2012)

[18] W.B. White, B.A. De Angelis, Spectrochim. Acta A 23, 985 (1967)

[19] G Bauer, W Richter, Optical characterization of epitaxial semiconductor layers, Springer-Verlag, Berlin, 1996

[20] H Zheng, J Kreisel, Y-H Chu, R. Ramesh and L. Salamanca-Riba, Appl. Phys. Lett. 90, 113113 (2007)

[21] P.D. Thang, G. Rijnders, D.H.A. Blank, J. Magn. Magn. Mater. 310, 2621 (2007)

[22] U. Netzelmann, J. Appl. Phys. 68, 1800 (1990)

[23] J. Dubowik, Phys. Rev. B 54, 1088 (1996)

[24] J. Dubowik, Phys. Rev. B 62, 727 (2000)

[25] F. Rustichelli, J.J. Skrzypek (Eds), Innovative Technological Materials: Structural Properties by Neutron Scattering, Synchrotron Radiation and Modeling, Chap. 4, Springer-Verlag, Berlin, (2010)

[26] V.G. Patil, Sagar E. Shirsathb, S.D. Morec, S.J. Shuklac, K.M. Jadhav, J. Alloys Compound, 488, 199–203 (2009)

Figure Captions

Figure 1: X-ray diffraction spectra measured on the $(PbNb_2O_6)_{1-x}$-($CoFe_2O_4)_x$ films with a) x = 90%, b) x = 50% and c) x = 10%, deposited with a target-substrate distance of 3 cm. In d) to f) are the spectra obtained on the films with x = 10% and target-substrate distances of 5 cm, 7 cm and 10 cm, respectively. The vertical lines (|) indicate the peak positions of the orthorhombic $PbNb_2O_6$ phase, the open circles (0) mark the corresponding ones for cubic $Pb_3Nb_4O_{13}$ and the losenges (♦) mark the peaks for $CoFe_2O_4$ with the cubic spinel structure.

Figure 2: On a) is the scanning electron microscopy (SEM) micrograph of the surface of the $(PbNb_2O_6)_{1-x}$-$(CoFe_2O_4)_x$ thin film, with x = 10%, deposited with d_{ST} = 9 cm. In b) is the histogram of the grain sizes, determined from the SEM micrographs of figure a).

Figure 3: Raman spectra of the $(PbNb_2O_6)_{1-x}$-($CoFe_2O_4)_x$ thin films with x = 10%, 30%, 50% and 70%. Also shown are the corresponding fitting curves, the $PbNb_2O_6$ and $CoFe_2O_4$ reference powders (x = 0% and x = 100%, respectively) and the Lorentzians obtained from the fit to the spectrum of the samples with x = 30 %.

Figure 4: Magnetization hysteresis cycles measured, at room temperature, on the thin film composites with cobalt ferrite concentrations of a) 30%, b) 40%, c) 50% and d) 70%, both for applied magnetic field parallel and perpendicular to the plane of the samples.

Figure 5: Anisotropy fields of the nanocomposite films with cobalt ferrite concentrations x = 10%, 40%, 50% and 70%. The curves are: H_A – experimental, H_σ - stress induced and H_d – due to the shape.

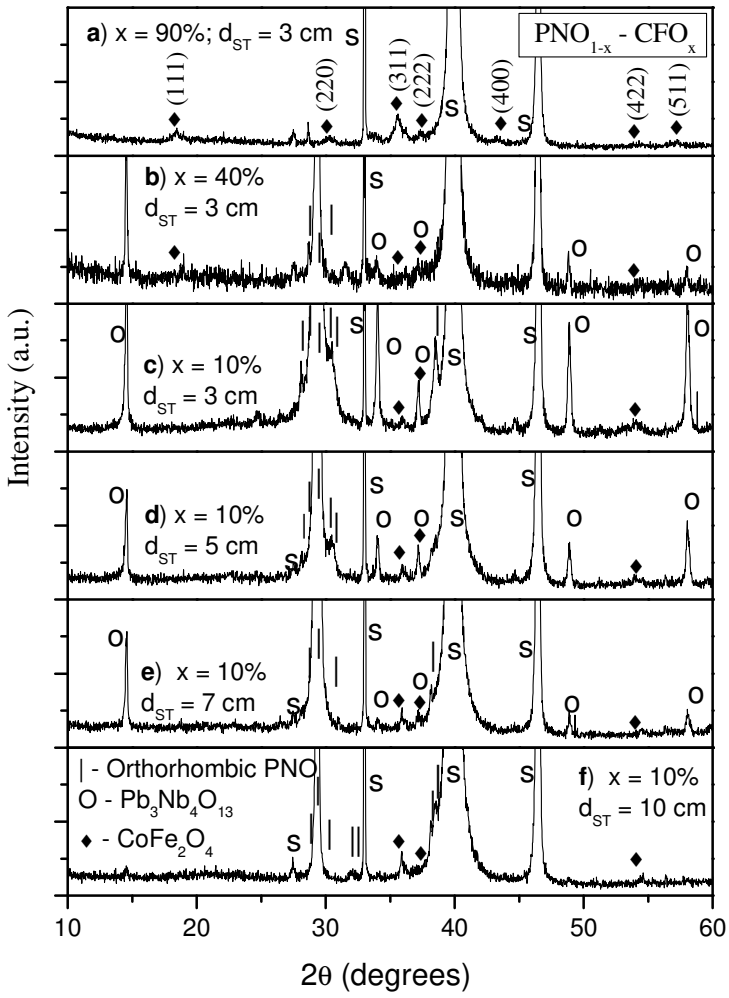
a) x = 90%; d_ST = 3 cm
PNO1-x - CFOx
(111)
(220)
(311)
(222)
(400)
(422)
(511)
b) x = 40%
d_ST = 3 cm
c) x = 10%
d_ST = 3 cm
d) x = 10%
d_ST = 5 cm
e) x = 10%
d_ST = 7 cm
f) x = 10%
d_ST = 10 cm
| - Orthorhombic PNO
O - Pb3Nb4O13
♦ - CoFe2O4
Intensity (a.u.)
2θ (degrees)
10
20
30
40
50
60

Figure 1

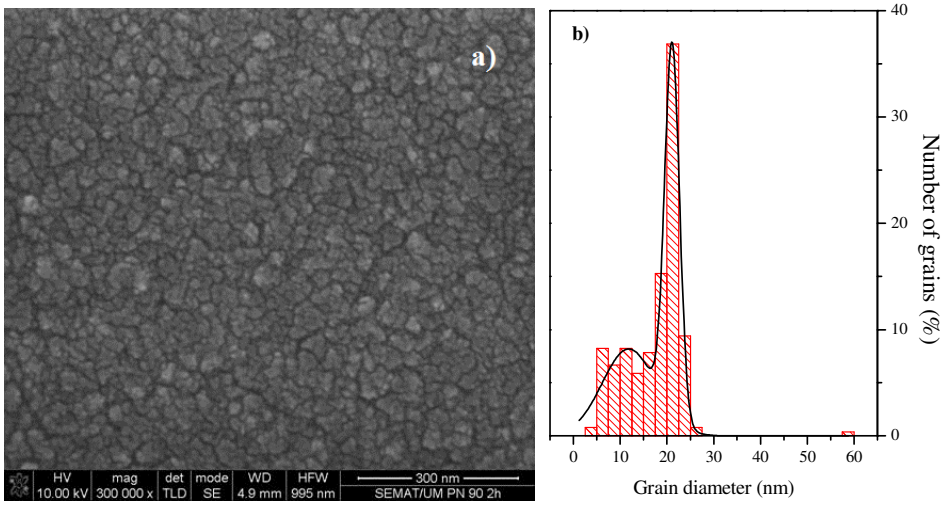
a)
HV
10.00 kV
mag
300 000 x
det
TLD
mode
SE
WD
4.9 mm
HFW
995 nm
300 nm
SEMAT/UM PN 90 2h
b)
Number of grains (%)
Grain diameter (nm)
0
10
20
30
40
50
60

Figure 2

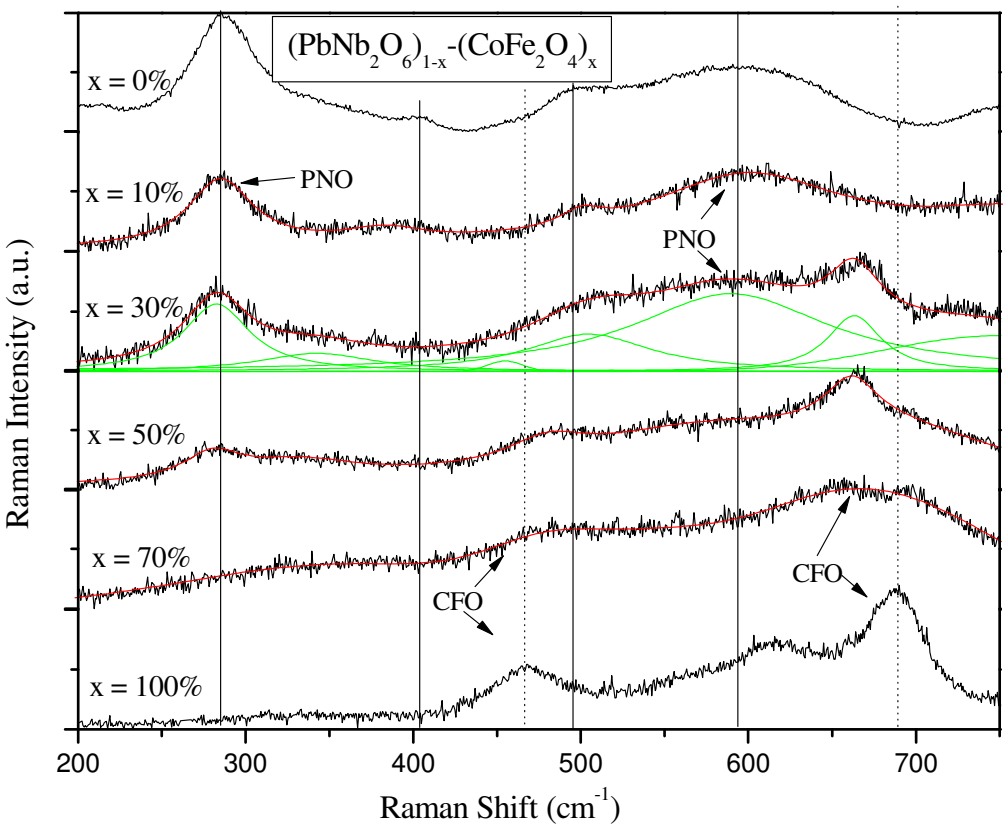
(PbNb2O6)1-x-(CoFe2O4)x
x = 0%
x = 10%
x = 30%
x = 50%
x = 70%
x = 100%
PNO
PNO
CFO
CFO
Raman Intensity (a.u.)
Raman Shift (cm-1)
200
300
400
500
600
700

Figure 3

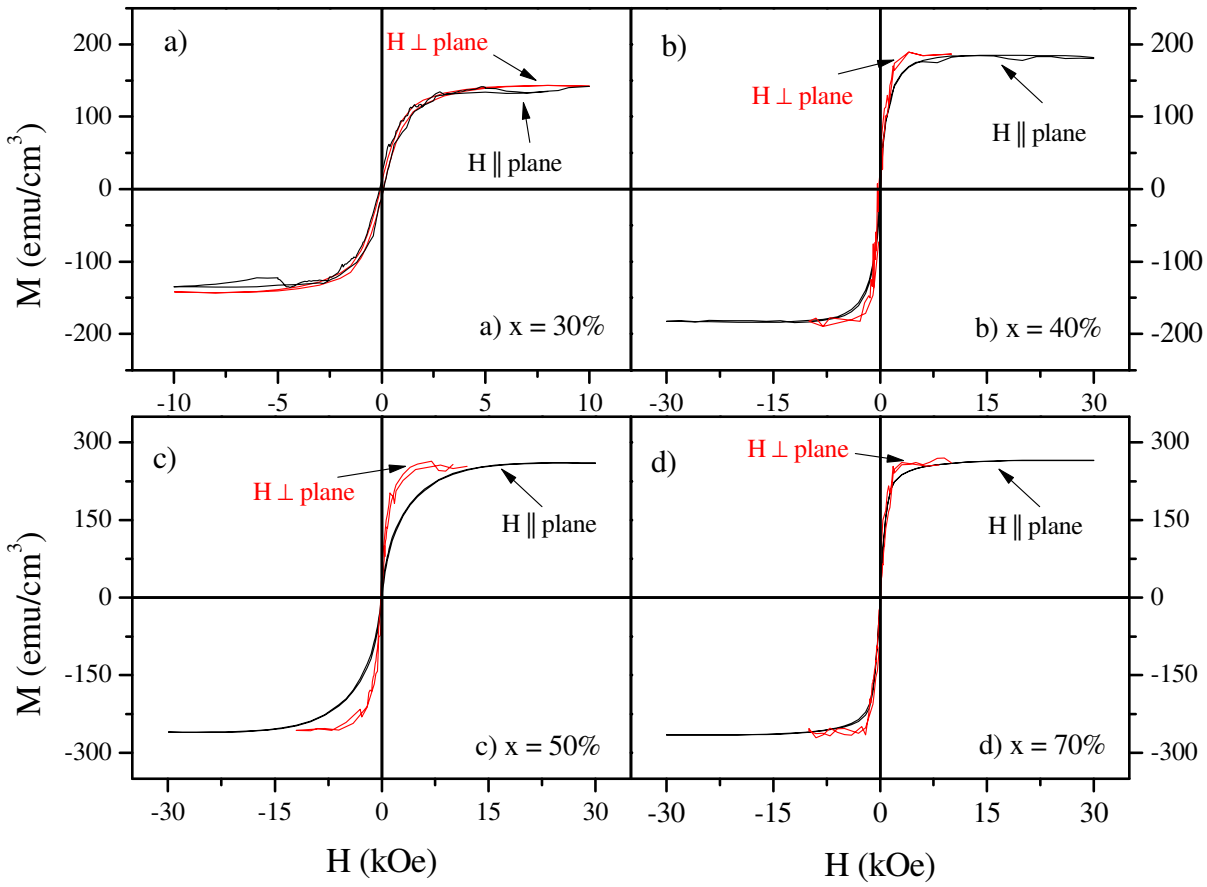
a)
H ⊥ plane
H ∥ plane
a) x = 30%
b)
H ⊥ plane
H ∥ plane
b) x = 40%
c)
H ⊥ plane
H ∥ plane
c) x = 50%
d)
H ⊥ plane
H ∥ plane
d) x = 70%
M (emu/cm3)
M (emu/cm3)
H (kOe)
H (kOe)

Figure 4

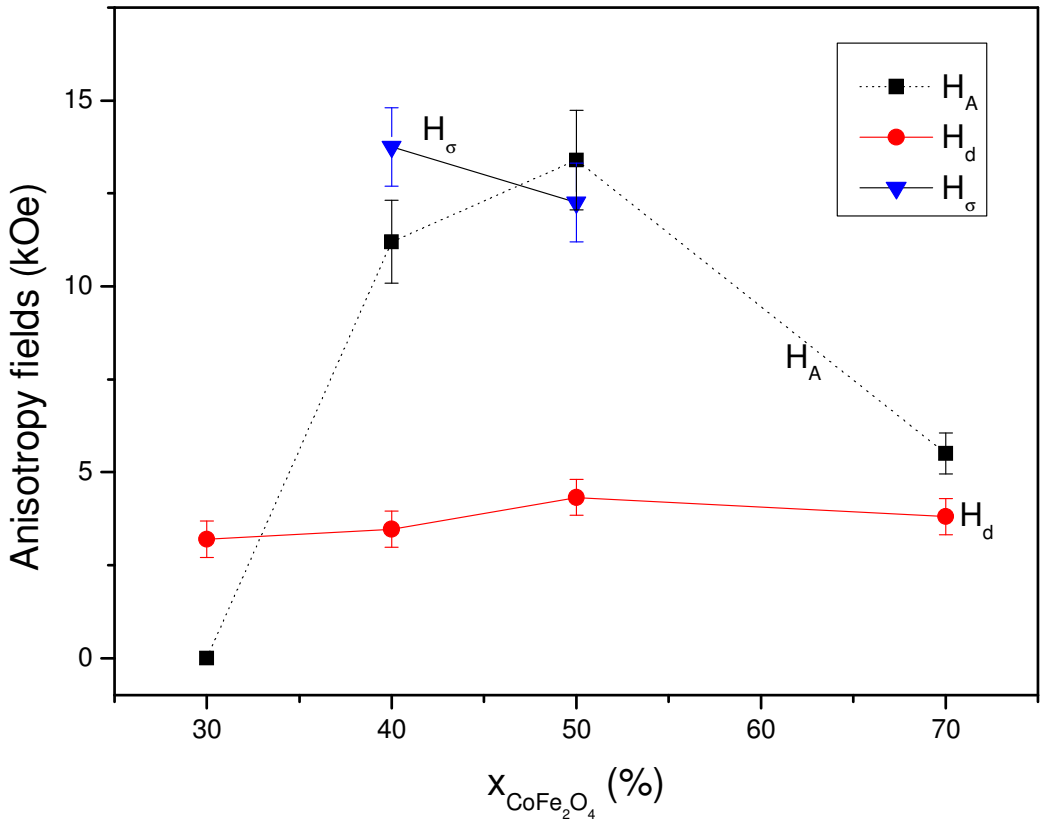
Anisotropy fields (kOe)
15
10
5
0
30
40
50
60
70
$x_{CoFe_2O_4}$ (%)
H_A
H_d
H_σ
H_σ
H_A
H_d

Figure 5